Bonding in skutterudites: Combined experimental and theoretical characterization of $CoSb_3$

I. Lefebvre-Devos,* M. Lassalle, and X. Wallart
IEMN, Département ISEN (UMR 8520 CNRS), 41 boulevard Vauban, 59046 Lille Cedex, France

J. Olivier-Fourcade, L. Monconduit, and J. C. Jumas
LAMMI (ESA 5072 CNRS), Université Montpellier II, place Eugène Bataillon, 34095 Montpellier Cedex 5, France
(Received 10 March 2000; revised manuscript received 22 June 2000; published 12 March 2001)

We report on the bonding in skutterudites using the $CoSb_3$ example. The theoretical electronic structure is calculated in both density-functional theory and empirical tight-binding frameworks. It is shown to be in good agreement with x-ray photoemission and photoabsorption experiments, and with ^{121}Sb Mössbauer spectroscopy. It is then used to demonstrate that (i) the Sb_4 rings are not the main structural features to analyze the highest valence-band behavior, (ii) the structure must be described in terms of corner-connected $CoSb_6$ octahedra, which are tilted to form the Sb rings.

DOI: 10.1103/PhysRevB.63.125110 PACS number(s): 71.20.−b, 82.80.Pv, 82.80.Ej

Skutterudites correspond to a large family of compounds of formula MP_3, where M is a transition metal (Ir, Co, or Rh) and P is a pnictide (P, As, or Sb). During recent years, they have been extensively studied as potential good thermoelectric materials. This property is mainly attributed to their good electrical conduction and poor thermal conduction characteristics (''electron-crystals and phonon-glasses'' concept[1]). This was attributed to two atomic structure particularities. (i) Large voids authorize the introduction of heavy atoms (rare-earth elements); this has been associated with a reduction in thermal conductivity. (ii) Pnictide rings have been shown to characterize the electronic states around the forbidden band gap and to be essential in the lattice-dynamics analysis.

Due to these potential applications, there is a great deal of interest in understanding their electronic structure. $CoSb_3$ is generally chosen as a reference material,[2–4] but, to our knowledge, there exists no direct experimental characterization of its electronic structure.

The aim of this work is to go further in understanding the $CoSb_3$ electronic structure and bonding. This aim is achieved by combining experimental and theoretical results. Among the experimental techniques used to study band structures, x-ray photoemission (XPS) and absorption (XAS) spectroscopies play a predominant part since they are particularly well suited for probing the valence- and conduction-band densities. XPS and XAS spectra are recorded. As they have to be compared to total and projected densities of states, which are not available in previous calculations, we have performed electronic-structure calculations by use of density-functional (DFT) and tight-binding (TB) theories. Lastly, ^{121}Sb Mössbauer spectra have been recorded in order to provide much insight into the antimony electronic structure.

We first recall (Sec. I) the $CoSb_3$ crystal structure and sample synthesis. In Sec. II, the techniques used for electronic-structure calculations are described and results are presented and compared to previous ones. Section III deals with the valence-band analysis. The XPS spectrum is analyzed with the help of theoretical densities of states (DOS) and photoionization cross sections. The conduction-band analysis is presented in Sec. IV. The XAS spectra are combined and compared to the theoretical projected conduction DOS. In the final section (Sec. V), we focus our attention on the antimony atom contribution to the electronic structure. It is first described by means of ^{121}Sb Mössbauer spectroscopy. Then, electronic density maps show their contribution to the bonding.

I. COMPOUND DESCRIPTION

A. Crystal structure

The $CoSb_3$ structure[5] is based on a bcc lattice (cell constant $a=9.0305$ Å) with four formula units per cell. The unit-cell symmetry corresponds to the space group $Im3$. Co atoms lie in the $8e$ position $(\frac{1}{4},\frac{1}{4},\frac{1}{4})$ and Sb atoms in the $24g$ position $(0,y=0.3351,\ z=0.1602)$. The main interactomic distances are reported in Table I.

Two kinds of description may be made. As will be seen in the final section (Sec. V), the first one is geometrically easy to describe as the second one takes bonding into account. Geometrically, the skutterudite structure [Fig. 1(a)] may be viewed as a simple cubic sublattice of Co atoms of basic cell with a dimension $a/2$. Six four-membered ''rings'' of Sb atoms are inserted in the cubes along the (100), (010), or (001) crystallographic directions, two cubes remaining vacant. The $CoSb_3$ structure [Fig. 1(b)] may also be considered as formed by corner-sharing $CoSb_6$ octahedra that are tilted in order that Sb atoms form the Sb_4 rings, which may be approximated to squares.

TABLE I. Crystallographic data: Bonding distances in $CoSb_3$ in Å .

	X-ray diffraction	Relaxed positions
Sb-Sb	2.978	2.939
	2.893	2.807
Co-Sb	2.519	2.470
Co-Co	4.517	4.424

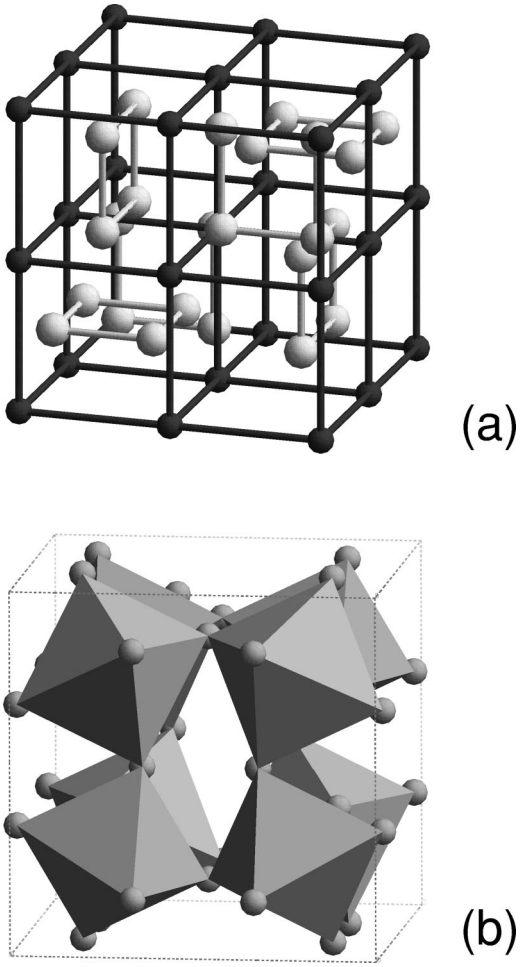

FIG. 1. $CoSb_3$ atomic structure viewed as (a) cubic cobalt (black atoms) units in which antimony (white atoms) rings are inserted or (b) $CoSb_6$ octahedral units.

B. Sample synthesis

The compounds were prepared by heating stoichiometric quantities of antimony powder (purity 99.5%, Aldrich) and cobalt powder (purity 99.995%, Aldrich) in evacuated, sealed quartz tubes. The binary sample was heated at 50 °C/h and maintained for one week at 750 °C and then crushed, reannealed for an additional week at 700 °C, and finally cooled to room temperature at 10 °C/h. The material was carefully handled throughout the preparation process to prevent unexpected contamination: it was handled in an argon-filled glove box. The purity of the sample was determined from x-ray powder analysis.

II. ELECTRONIC-STRUCTURE CALCULATION

Let us briefly summarize here the previous calculations of the skutterudite electronic structure. A chemical picture was first given by Jung *et al.*[2] They pointed out that the highest occupied band of LaF_4P_{12} has mainly a $P(3p)$ character. They analyze this in terms of P_4 atomic squares. The *ab initio* calculation performed by Singh and Pickett[3] used the experimental crystal structure and an extended-potential linearized augmented-plane-wave method (LAPW). They focused on the highest occupied band at the Γ point. It displays a quasilinear dispersion. Although the $CoSb_3$ band structure was drawn, no density of states is reported. The work of Sofo and Mahan[4] also reports an LAPW calculation but it was performed at the relaxed positions (those sumitted to zero force). The forbidden band-gap value is different from those obtained by Singh and Pickett. This was related to the difference in antimony positions and thus to the Sb_4 rings. This work shows a density of states (DOS) but no longer projected ones.

As we will calculate electron density maps and will need the projected DOS, we also have to calculate the $CoSb_3$ electronic structure. For our purpose, we use two techniques. The first one is carried out within the density-functional-theory (DFT) framework[6,7] using the local-density approximation (LDA), a plane-wave basis, and ultrasoft pseudopotentials. It is implemented in the Cerius2 environment (CASTEP code).[8] This calculation is performed at the relaxed positions (variation in the lattice constant of 2% for a, and 0.3% and 1%, respectively, for y and z of the 24g Sb crystallographic site). The CASTEP results will further enable us to draw the charge-density maps (Sec. V). The second approach is the semiempirical tight-binding method (TB), in which parameters are fitted in order to reproduce the main characteristics of the *ab initio* band structure.[9] The minimal basis used in TB is reduced to 5s and 5p orbitals for antimony atoms and 3d ones for cobalt atoms (4s are shown to have no influence on the description of the valence and low conduction bands). The TB results will then allow us to relate regions of the DOS to atomic levels, which is required to compare calculated DOS and XPS x-ray-absorption near-edge spectroscopy (XANES) spectra (Sec. III and Sec. IV).

Due to the well-known problem of underestimation of the gap by the LDA, it is difficult to predict a value for the band gap. Nevertheless, the gap is increased when the atomic positions are relaxed (from 0.195 to 0.330 eV). But this does not mean a particular sensitivity to Sb rings as all distances are varied during the relaxation (see Table I). Our band structure also shows unusual behavior near the Fermi level described by Singh[3] and Sofo.[4] Using the two-band Kane model

$$\frac{\hbar^2 k^2}{2m^*} = \epsilon_k \left(1 + \frac{\epsilon_k}{A} \right) \tag{1}$$

(where $\hbar$ is the reduced Planck constant, k is the wave vector, m^* is the effective mass, ϵ_k is the energy band, and A is a constant term), we fit our LDA results and obtain an effective mass $m^* = 0.08 m_0$ and $A = 0.25$ as Sofo obtained $m^* = 0.07 m_0$ while fixing A to 0.22 eV. The DOS from our calculations and those of Sofo are compared in Fig. 2. There is an overall agreement between them. Let us detail this. Concerning the valence band, two main structures A and B that are similar in width are noticed. Nevertheless, some discrepancies appear in B substructures. (i) All results show a main peak Bd that is higher in energy in the TB result. (ii) One may assume a substructure $B1$ between -4 and -6 eV. (iii) Another substructure $B2$ clearly exists in the first-principles calculations around -3 eV. Due to XPS experi-

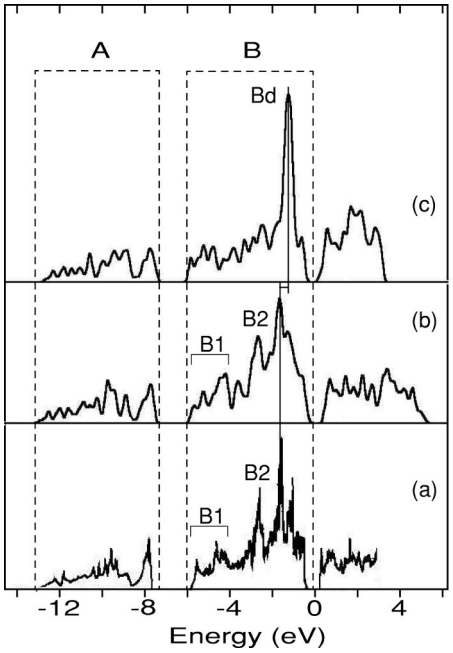

FIG. 2. $CoSb_3$ calculated density of states obtained (a) in LAPW, (b) with CASTEP code, and (c) in the tight-binding framework with our fitted parameters.

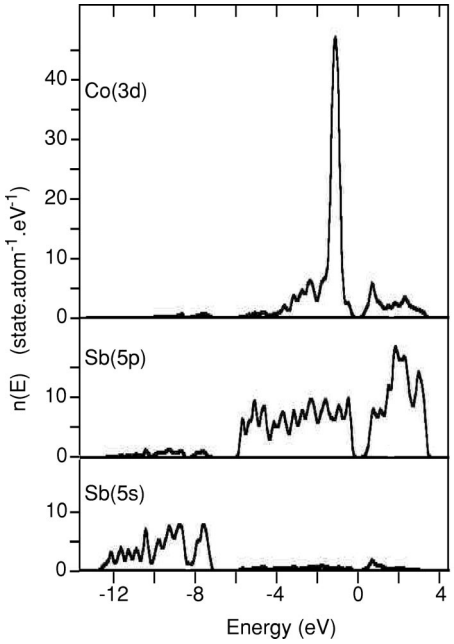

FIG. 3. $CoSb_3$ projected density of states obtained in the tight-binding framework.

mental resolution and the approximation described in the next section, one may expect from XPS to well reproduce the A and B width and the $B1$, $B2$, and Bd position relative to the valence-band top. With regard to the conduction band, methods are not devoted to describe states on a large energy range. Particularly, the TB one is known to only give a good description of the bottom of the conduction band (due to the use of a minimal basis set). One expects from XANES spectra to confirm the bottom of the conduction band and give information on higher-energy states.

Our CASTEP electronic structure is in good agreement with the previous ones and can be used to go further in the analysis of bonding. The TB fit is sufficiently good to make use of the corresponding projected DOS to compare our calculations to experimental results and to analyze the various contributions to the electronic structure.

III. VALENCE-BAND CHARACTERIZATION

We first analyze the valence band of $CoSb_3$. The projected DOS obtained in the TB framework are represented in Fig. 3. They clearly show that structure A is mainly due to Sb(s) states and structure B is due to interactions between Sb(p) and Co(d) states. The Bd peak is due to Co(d) states and the highest valence bands have mainly an Sb(p) character.

XPS spectra of $CoSb_3$ samples have been recorded on a model 5600 spectrometer from Physical Electronics using a monochromatic Al $K\alpha$ x-ray source and a pass energy of 11.75 eV. In these conditions, the energy resolution as measured from the full width at half-maximum (FWHM) on the Ag $3d5/2$ line is 0.55 eV. The binding-energy scale has been calibrated using the Au $4f7/2$ line at 84.0 eV. The acceptance angle of the analyzer has been set to 14° and the angle between the surface plane and the analyzer axis is 75°.

The XPS spectrum should be compared to a recomposition $N(E)$ of the valence-band DOS taking photoionization cross sections into account through the formula

$$N(E)=\sum_i n_i(E)\sigma_i, \tag{2}$$

where the sum stands over the projected contributions, $n_i(E)$ are the projected DOS of character i, and σ_i is the corresponding cross sections of atoms in the crystal. As it is not the aim of this paper to calculate the crystalline σ_i, they are approximated to those of free atoms.[10] This generally allows the influence of the σ_i to be correctly reproduced and to have a correct estimate of $N(E)$. The resulting $N(E)$ is compared to the XPS spectrum in Fig. 4. Structures A and B are well reproduced in shape and width. Even detailed peaks Bd, $B1$, and $B2$ are reproduced. The correct position of Bd, which is also noted in our TB calculations, indicates a good description of the highest valence states.

IV. CONDUCTION-BAND CHARACTERIZATION

In the case of x-ray-absorption spectroscopy, emphasis lies on the accessibility of the dipole selected transitions to the s, p, and d orbitals from a suitable inner level. For example, the transitions from an inner p level scan the s and d symmetry orbitals in the conduction band. It is thus particularly well suited to get insight into the partial densities of unoccupied states. We have performed the x-ray-absorption near-edge spectroscopy at the LURE laboratory (Orsay) on the DCI storage ring. The accessible energies between 4 keV and 20 keV allow the use of transition-metal K edges and antimony L edges. We present here the Sb L_I, Sb L_{II}, and

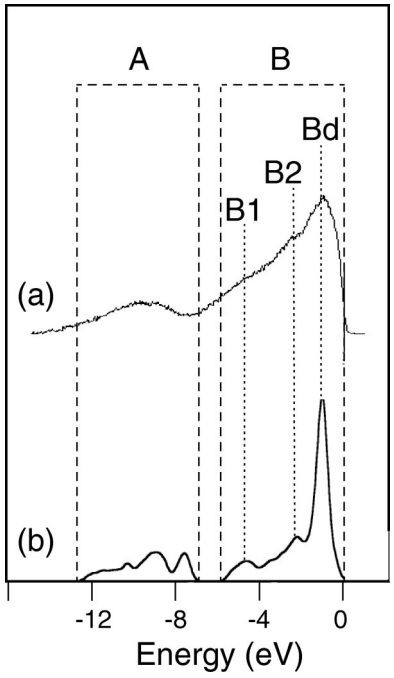

FIG. 4. $CoSb_3$ (a) XPS spectrum after standard background substraction compared to (b) the theoretical recomposition from the projected DOS.

Co K XANES spectra of $CoSb_3$. The sample was finely ground and passed through a 5-μm sieve in order to obtain powders being homogeneous in particle size. A thin membrane was coated with this powder. The recordings were carried out in the transmission mode. The beam line was equipped with a Si(311) two-crystal monochromator for the Co K edge allowing a resolution of 0.2 eV and with a Si(111) monochromator for the Sb L edges. Energy calibration was carried out, respectively, from the standard spectra at the Ni K edge of a high-purity Ni foil (8333 eV) and at the Ti K edge of TiO_2 (prepeak at 4967.5 eV). The XANES spectra were treated in the following way. First, the absorption background was subtracted supposing a linear behavior over the whole energy range. Then the spectra were normalized to give the same absorption step amplitude in a range of pure atomic absorption.

The XANES spectra may be split in two regions, namely the close near-edge and the post-edge region (from $\sim$15 eV to 70 eV above the threshold). The second is generally modeled taking the multiple scattering of photoexcited electrons into account. The near edge is generally analyzed in terms of electronic transitions to empty states, assuming a weak perturbation due to the core-hole creation. It has been demontrated that this is negligible in metals.[11] In $CoSb_3$, we consider that there is a sufficient number of valence electrons on each atom to assume a good screening of the core hole. Thus, spectra are interpreted as the ground-state electronic structure of the conduction band.

The XANES spectra are reported in Fig. 5. The Co K spectrum gives an experimental view of the Co(p) conduction states (transition $1s \rightarrow 4p$). It mainly exhibits two peaks a and b. The existence of peak a is confirmed by the two inflection points labeled a' and b'. The Sb L_I spectrum

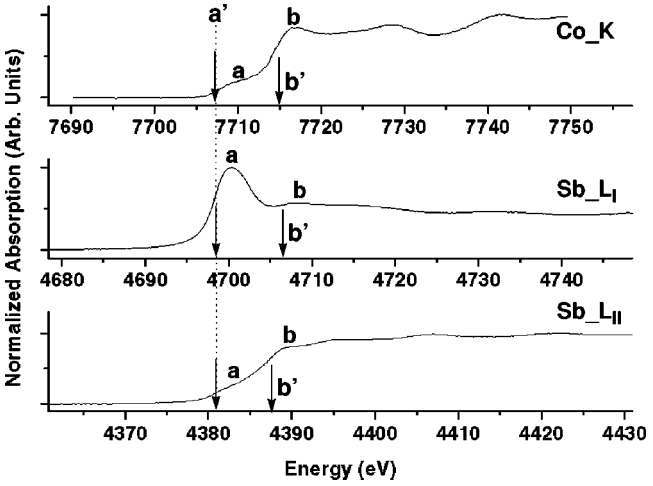

FIG. 5. $CoSb_3$ XANES spectra at the Co K edge, Sb L_I edge, and Sb L_{II} edge. Arrows indicate the first derivative peak position. They are superposed in order to align a' first derivative peaks.

scans the Sb(p) conduction states (transition $2s \rightarrow 5p$) and shows a structure (labeled a) of which the full width at half maximum is measured to be 4.2 eV. It is related to the bottom of the conduction band (see Fig. 3). Its theoretical width (3.6 eV) is in agreement with the experimental one when the experimental enlargement is taken into account. Considering the Sb L_{II} spectrum, the Sb(s) and Sb(d) conduction states are described (transition $2p \rightarrow 5s$, $5d$). Its a' and b' first derivative peaks also confirm the existence of the prepeak labeled a. The electronic-structure calculations (Fig. 3) show that it corresponds to Sb($5s$) states. Let us compare them here to XANES Sb L_{II} spectra recorded for various antimony chalcogenides, in which Sb is characterized by a lone pair.[12] In that case, due to the valence Sb($5s$) lone pair (the corresponding theoretical population is greater than 1.9 electrons), there is a very weak antibonding contribution of the Sb($5s$) states to the conduction band. Nevertheless, the Sb($5s$) conducting population in $CoSb_3$ is calculated to be 0.23 electron, which is greater than the maximum 0.1 electron in Sb lone-pair chalcogenides. As the corresponding peak is less intense in the spectra, we think that the Sb($5s$) electrons are delocalized and spread in the conduction band; they do not participate in an antibonding state.

These XANES spectra can be superimposed on a common energy scale to obtain a complete picture of the conduction-band DOS. This approach extends the identification to higher vacant electronic states.[13] To align spectra, a method may consist of subtracting the binding energy of the free atom core (Co K=7709 eV, Sb L_I=4698 eV, and Sb L_{II}=4380 eV).[14] One may see in Fig. 5 that this would lead to taking the a' peak as zero energy on Sb spectra as this a' peak would have a slighly negative energy (~ -1 eV) in the Co spectrum. We assume that this weak energy shift between a' peaks is due to the approximative binding energies, which are different in free atoms and atoms in compounds. Thus, we prefer here to align the a' peaks of each spectrum. This peak is taken as the origin of the energy scale. The superposition of spectra is shown in Fig. 5. The coincidence of peaks b', a, and b enables a description of the conduction states in

the following way. (i) A first peak whose major character is Sb(p). Sb(s) states participate weakly as they are spread in the conduction band. Co(p) states also weakly participate. (ii) A second peak mainly due to Co(p)-Sb(d) interaction, which we attribute to the octahedral $CoSb_6$ environment. Its energy position is similar to those in the CoS_2 compound. Its width is consistent with a strong angular distorsion of the Co-Sb bonds.

V. ANTIMONY CONTRIBUTION

As previously pointed out, it seems that the electronic structure of skutterudites is generally related to the Sb_4 rings. Thus, we focus on the antimony bonding by two means: (i) the ^{121}Sb Mössbauer spectroscopy, which scans the electronic local environment of antimony atoms; (ii) our electronic calculations, which have been demonstrated to be in good agreement with experimental XPS and XANES spectra.

A. Mössbauer spectra

Mössbauer spectroscopy enables the study of solids on an atomic scale. Spectra are mainly characterized by two parameters: the isomer shift (δ) and the quadrupolar splitting (Δ). The first one corresponds to the peak position in the spectrum. It may be written as

$$\delta = \mathcal{N}[|\Psi_a(0)|^2 - |\Psi_s(0)|^2], \tag{3}$$

where $\mathcal{N}$ is a nuclear prefactor and $|\Psi(0)|^2$ reflects the electronic density at the probe nucleus. This density can be considered as proportional to the Sb($5s$) electrons in the valence band.[15] The second corresponds to the peak splitting. This splitting is induced by the electric-field gradient and thus it is related to the local environment distortion. Its analysis lets one build up a picture of the symmetry of the electron distribution close to the probed nucleus.

^{121}Sb Mössbauer measurements were performed in a standard transmission geometry using a ^{121m}Sn in a $BaSnO_3$ source of nominal activity 0.5 m Ci on a constant acceleration spectrometer. During the measurements, both source and absorber were simultaneously cooled down to liquid-helium temperature to increase the fraction of the recoil-free absorption and emission process. An absorber was prepared from powder mixed with A-piezon grease (15 mg of antimony/cm^2). The velocity scale was calibrated with the standard spectrum of an iron absorber obtained using a ^{57}Co(Rh) source. The zero isomer shift was defined from the spectrum of InSb at 4 K [$\delta=0$ mm/s, $\Delta=0$ mm/s, and $\Gamma=1.65(5)$ mm/s with $\delta=-8.76(4)$ mm/s relative to the $Ba^{121m}SnO_3$ source]. Data were fitted using transmission integral analysis software GM5SIT.[16] The Mössbauer source fraction f and source linewidth Γ were held constant at 0.62 and 1.45 mm/s, respectively.

The Mössbauer spectrum is shown in Fig. 6. A principal broad asymmetric absorption is observed that ranges between -6 and -15 mm/s relative to the source and indicating an unresolved quadrupole spectrum. The weak absorption ($<2\%$) near 0 mm/s is attributed to an accidental

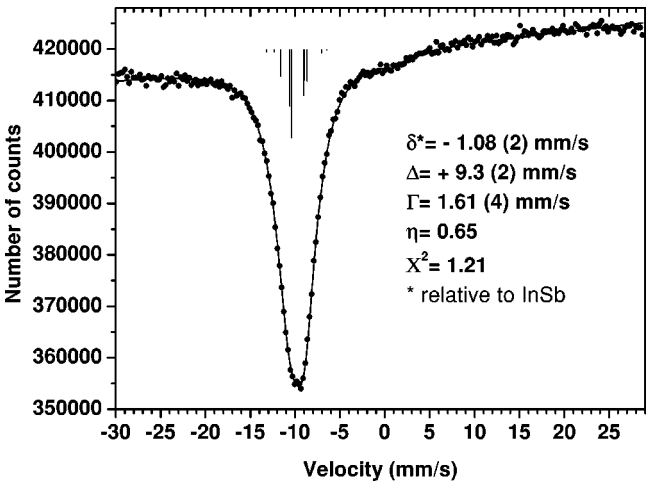

FIG. 6. ^{121}Sb Mössbauer spectrum of $CoSb_3$.

oxidizing of the sample (impurity of Sb_2O_5). Mössbauer parameters $\delta=-1.08(2)$ mm/s relative to InSb, $\Delta=+9.3(2)$ mm/s, $\eta=0.65(2)$, and $\Gamma=1.61(4)$ mm/s are in good agreement with previous data[17] ($\delta=-0.96$ mm/s relative to InSb, $\Delta=+9.0$ mm/s, $\eta=0.98$, and $\Gamma=1.8$ mm/s). By comparison with the natural linewidth emission ($\Gamma_r=1.24$ mm/s),[16] the observed linewidth ($\Gamma=1.61$ mm/s) quite agrees with only one crystallographic Sb environment in accordance with the crystal structure. The measured isomer shift, $\delta=-1.08(2)$ mm/s relative to InSb, is in agreement with an Sb($5s$) electronic population to be 1.77 electron in our TB model. As compared to the reference isomer shift scale,[18] this situation is intermediate between an active lone-pair situation and that of InSb, where the Sb($5s$) electrons are engaged in covalent bonds. It is in agreement with our previous interpretation of the prepeak a in Sb L_{II} XANES spectra. The large value of quadrupole splitting ($\Delta=+9.3$ mm/s) and the $\eta=0.65$ factor suggest a strongly distorted environment. It corresponds to the geometrical distortion of the Sb(Co_2,Sb_2) tetrahedra and to the chemical difference in the antimony neighbors (Co and Sb).

We also make use of the CASTEP electronic stucture to study the geometrical distribution of the Sb($5s$) electrons in the $CoSb_3$ compound. A charge-density map of valence electrons in the -14 to -7 eV energy range is reported in Fig. 7. It is shown that there is no lone-pair activity (in agreement with the isomer shift) because there is no electron cloud detached from the Sb nucleus in a given direction. But the isodensity is not spherical (in agreement with a strong quadrupole splitting). The distorsion is along the direction of Sb neighbors, due to participation in the Sb-Sb bonding.

B. Bonding

The Sb bonding can be analyzed by means of charge-density maps obtained from CASTEP results. We first examine the highest occupied band. The projected DOS (Fig. 3) have shown that it mainly comes from Sb($5p$) states. The corresponding charge-density map is reported in Fig. 8. The important point is that the density is not situated on the Sb_4 ring or Sb-Sb bonding [Fig. 8(a)]. The charge density is topologi-

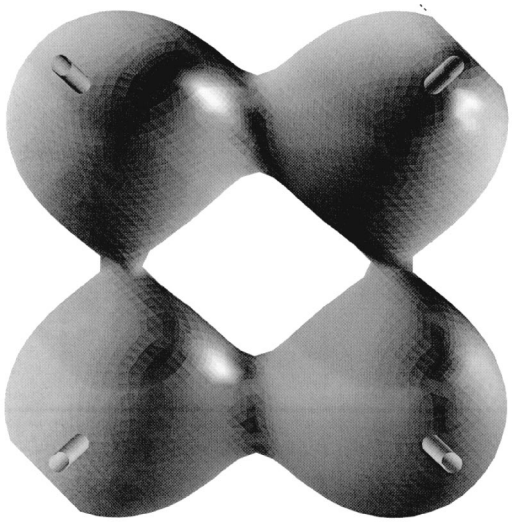

FIG. 7. $CoSb_3$ charge-density map derived from CASTEP of valence Sb($5s$) electrons around antimony atoms. The isodensity value is 0.095 electron/Å^3.

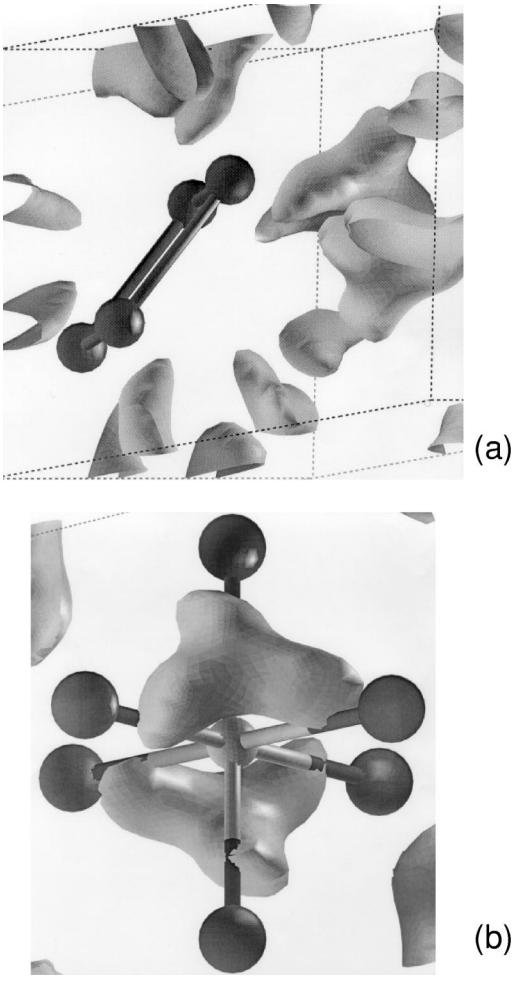

FIG. 8. $CoSb_3$ charge-density map derived from CASTEP of the highest valence band. The isodensity value is 0.025 electron/Å^3. Views are centered on (a) an Sb_4 ring and (b) a $CoSb_6$ octahedron.

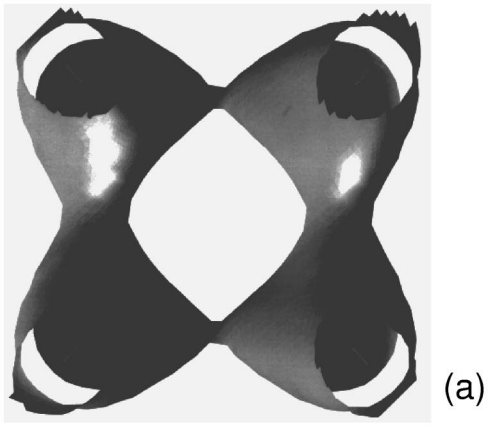

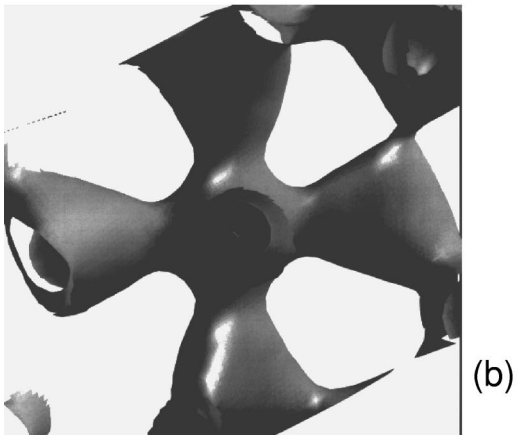

FIG. 9. $CoSb_3$ charge-density map derived from CASTEP of the whole valence band. The isodensity value is 0.33 electron/Å^3. Views are centered on (a) an Sb_4 ring and (b) a $CoSb_6$ octahedron.

cally included in the $CoSb_6$ octahedra [Fig. 8(b)]. Thus, even if the main character of the DOS is Sb($5p$), there is an interaction with Co($3d$) electrons and one cannot consider that the highest valence band is only concerned with the Sb_4 rings.

The whole valence-band charge density will now complete our bonding description. The corresponding map is reported in Fig. 9. The top view is centered on an Sb_4 ring. Its rectangular form leads to a stronger bonding on the short Sb-Sb bonds. The Sb-Sb bonding mainly comes from the *A* part of the DOS (compare to Fig. 3). In this view, the Co-Sb bonds are clipped. The bottom view clearly shows the Co-Sb bonding in the $CoSb_6$ octahedron (the front and back Co-Sb bonds are clipped for the sake of clarity). The Co-Sb bonds are equivalent and mainly come from the *B* part of the DOS. The Sb-Sb and Sb-Co bonding characters are qualitatively similar. Thus, from an electronic point of view, one cannot describe the structure by means of rings inside a cubic cobalt structure or by means of independent $CoSb_6$ units.

VI. CONCLUSION

We have calculated the $CoSb_3$ electronic structure and obtained the band structure, the total and projected densities

of states. The band structure has been shown to be in agreement with previous ones. The valence band density of states has been successfully compared with the recorded x-ray photoemission spectra. In particular, it shows that the first valence-band maximum [corresponding to Co($3d$) states] is situated nearer the valence-band top than previously expected. The conduction densities of states have been examined by means of near-edge x-ray-absorption spectra. The superposition of these absorption spectra is also in good agreement with our electronic-structure calculation.

We have first focused bonding analysis on antimony. Its local electronic structure has been first described by Mössbauer spectrocopy. Correlated with the Sb($5s$) charge density maps, it was demonstrated that it is more convenient to consider Sb(Co_2,Sb_2) tetrahedra to describe the bonding. Going further in the charge density map exploitation, we have explained that the highest valence band [major Sb($5p$)] has not only a Sb_4 rings character. We have also shown that Sb-Sb and Co-Sb bonding characters are similar. Then we conclude that from the bonding point of view, the $CoSb_3$ atomic structure must be described as $CoSb_6$ connected by corners in order to form Sb_4 rings.

ACKNOWLEDGMENT

The authors thank Robert Cortes for his help in collecting data of DCI experiments at LURE (Orsay, France).

*Electronic address: Isabelle.Devos@isen.fr

[1] G. A. Slack, *Solid State Physics: Advances in Research and Applications*, edited by H. Ehrenreich, F. Seitz, and D. Turnbull (Academic, New York, 1979), Vol. 34.
[2] D. Jung, M.-H. Whangbo, and S. Alvarez, Inorg. Chem. **29**, 2252 (1990).
[3] D. J. Singh and W. E. Pickett, Phys. Rev. B **50**, 11 235 (1994).
[4] J. O. Sofo and G. D. Mahan, Phys. Rev. B **58**, 15 620 (1998).
[5] R. W. G. Wyckoff, *Crystal Structure* (Interscience, New York, 1948).
[6] P. Hohenberg and W. Kohn, Phys. Rev. **136**, B864 (1964).
[7] W. Kohn and L. J. Sham, Phys. Rev. **140**, A1133 (1965).
[8] Cerius2 User Guide, October 1995, San Diego:MSI (1995).
[9] I. Lefebvre, M. A. Szymanski, J. Olivier-Fourcade, and J. C. Jumas, Phys. Rev. B **58**, 1896 (1998).
[10] J. H. Scofield, J. Phys. Chem. Ref. Data **8**, 69 (1979).
[11] J. E. Müller, O. Jepsen, and J. W. Wilkins, Solid State Commun. **42**, 365 (1982).
[12] J. Olivier-Fourcade, P. E. Lippens, J.-C. Jumas, M. Womes, I. Lefebvre, M. Lannoo, J. M. Esteva, and R. C. Karnatak, Eur. J. Solid State Inorg. Chem. **30**, 139 (1993).
[13] M. Womes, R. C. Karnatak, J. M. Esteva, I. Lefebvre, G. Allan, J. Olivier-Fourcade, and J. C. Jumas, J. Phys. Chem. Solids **58**, 345 (1997).
[14] A. Bearden and A. F. Burr, Rev. Mod. Phys. **39**, 125 (1967).
[15] I. Lefebvre, M. Lannoo, G. Allan, A. Ibanez, J. Olivier-Fourcade, J. C. Jumas, and E. Beaurepaire, Phys. Rev. Lett. **59**, 2471 (1987).
[16] T. C. Gibb, *Principles of Mössbauer Spectroscopy* (Chapman and Hall, London, 1976), Vol. 18.
[17] A. Kjekshus, D. G. Nicholson, and T. Rakke, Acta Chem. Scand. **27**, 1315 (1973).
[18] J. Olivier-Fourcade, A. Ibanez, J. C. Jumas, M. Maurin, I. Lefebvre, P. Lippens, M. Lannoo, and G. Allan, J. Solid State Chem. **87**, 366 (1990).